Ionics (2018) 24:73–81
DOI 10.1007/s11581-017-2188-5

ORIGINAL PAPER

# Synthesis and electrochemical performance of carbon-coated $LiMnBO_3$ as cathode materials for lithium-ion batteries

**Wei Chen[1] · Hua Zhang[2] · Xiaoping Zhang[3] · Ling Wu[3] · Jiequn Liu[3] · Shijun Liu[1] · Shengkui Zhong[3]**

Received: 28 March 2017 / Accepted: 6 June 2017 / Published online: 28 June 2017


**Abstract** Carbon-coated $LiMnBO_3$/C is synthesized by a sol-gel method using polyethylene glycol 6000 (PEG-6000) as carbon source. The influences of different sintering temperatures on the crystal structure, morphology, and electrochemical performance of $LiMnBO_3$/C composites are investigated. XRD results indicate that the samples consist of the monoclinic phase $LiMnBO_3$ (m-$LiMnBO_3$) and the hexagonal phase $LiMnBO_3$ (h-$LiMnBO_3$), and the amount of m-$LiMnBO_3$ is reduced and the h-$LiMnBO_3$ is increased with the increasing sintering temperature. The particle size of the samples is about 500 nm, and the surface of the particles is coated with a thick amorphous carbon layer. The $LiMnBO_3$/C synthesized at 750 °C exhibits the initial discharge capacities of 213.4, 170.8, and 109.7 mAh $g^{-1}$ at 0.025, 0.05, and 0.5 C rates, respectively, and shows better cycling performance than that of bare $LiMnBO_3$. The enhanced electrochemical performance might be largely attributed to the uniformly coated carbon layers from decomposition of the PEG-6000.

**Keywords** Li-ion batteries · Cathode materials · $LiMnBO_3$ · Sol-gel method

✉ Shijun Liu
shijunliu@csu.edu.cn

✉ Shengkui Zhong
zsk_suda@163.com

[1] College of Chemistry and Chemical Engineering, Central South University, Changsha 415000, People's Republic of China

[2] Shanghai Shanshan Technology Co. Ltd., Shanghai 201209, People's Republic of China

[3] School of Iron and Steel, Soochow University, Suzhou 215021, People's Republic of China

## Introduction

Borate-based materials ($LiMBO_3$, $M$ = Mn, Fe, and Co) were first reported by Legagneur which have received wide attention in the research area of Li-ion batteries, since $LiMBO_3$ materials provide high theoretical capacity, high thermal stability, and good electrochemical stability because of small volume changes compared to other cathode materials [1–4]. In addition, $(BO_3)^{3-}$ polyanion could afford a high operating voltage along with an improved structural stability due to the inductive effect of B–O bond. Among the borates, $LiMnBO_3$ has a higher operation potential and a higher theoretical specific energy, which is a more promising candidate for lithium-ion batteries. $LiMnBO_3$ has two different crystal structures, the monoclinic phase and the hexagonal phase [5–9]. The two phases of $LiMnBO_3$ have the same theoretical capacity of 220 mAh $g^{-1}$, while due to their different crystal structure, the average potential for the monoclinic phase is 3.7 V and the hexagonal phase is 4.1 V [10–14].

However, $LiMnBO_3$ has intrinsically low electronic and ionic conductivity which is the main cause of the poor electrochemical performance of $LiMnBO_3$. Additionally, $LiMnBO_3$ is sensitive to moist air, which can induce both partial $Mn^{2+}$ oxidation and $Li^+$ loss from the crystal framework, and resulting in the reduce of the electrochemical activity. Thus, many strategies have been made to enhance the performance of $LiMnBO_3$ cathode materials, for instance, doping with metal ions, coating with carbon [15–18]. In these methods, carbon coating may be an effective way, which can improve the structure stability and enhance the cycle performance of $LiMnBO_3$ materials when it encounters with moist air and electrolyte [19–23]. Various polymers are already used as additives or carbon sources for cathode materials, such as polyethylene glycol (PEG), polystyrene, polyvinyl alcohol, polyaniline, and polypyrrole [24–28]. Among these polymers,

PEG is widely used in electrochemical and biomedical fields owing to its lubricity, nontoxicity, hydrophilicity, and solubility. As a dispersing agent and surfactant, PEG can be easily adsorbed onto the surfaces of particles by the ordered and uniform chain structure, effectively inhibiting the aggregation of colloidal particles in the process of gel formation, and playing the role of carbon source during sintering [29].

Herein, $LiMnBO_3$/C was prepared using a sol-gel method with PEG as the reductive agent and carbon source. We used PEG-6000 as carbon source, which serves multiple purposes: first, as a dispersant and surfactant, PEG can be easily adsorbed onto the surfaces of particles by the ordered and uniform chain structure during the formation of the gel; second, the formed particles are coated by the carbon produced by PEG decomposition during heat treatment, the in-situ coated carbon controls the growth of $LiMnBO_3$ particles; and last, the carbon coating can improve the conductivity of $LiMnBO_3$ materials and prevent $LiMnBO_3$ from air corrosion. Meanwhile, electrolyte adsorption in amorphous carbon layer also provided a flexible structure against volume expansion/contraction during the cycling progress [30–32].

## Experimental

### Synthesis of $LiMnBO_3$/C

The stoichiometric amount of $LiOH{\cdot}H_2O$ (AR, 95%), $Mn(CH_3COO)_2{\cdot}4H_2O$ (AR, 99%), and $H_3BO_3$ (AR, 99.5%) was dissolved in deionized water. In the same way, the demand amount PEG-6000 (CP) (the weight ratio of PEG and product $LiMnBO_3$/C is 1:2) was dissolved in deionized water. Then, the two solutions were mixed and stirred spiritedly at 80 °C until the homogeneous gel was obtained. Then, the gel was dried at 120 °C for 24 h in a vacuum oven. At last, the obtained powders were sintered at 350 °C for 3 h in argon atmosphere and then ball-milled for 1 h to minimize the particle size, subsequently, at 650–800 °C for 10 h in argon atmosphere to obtain $LiMnBO_3$/C powders.

### Synthesis of bare $LiMnBO_3$

The bare $LiMnBO_3$ was prepared in the above synthetic process; the stoichiometric amount of $LiOH{\cdot}H_2O$ (AR, 95%), $Mn(CH_3COO)_2{\cdot}4H_2O$ (AR, 99%), and $H_3BO_3$ (AR, 99.5%) was dissolved in deionized water. Then, the solution was stirred spiritedly at 80 °C until the homogeneous gel was obtained. Then, the gel was dried at 120 °C for 24 h in a vacuum oven. At last, the obtained powders were sintered at 350 °C for 3 h in argon atmosphere and then ball-milled for 1 h to minimize the particle size, subsequently, at 750 °C for 10 h in argon atmosphere to obtain $LiMnBO_3$ powders.

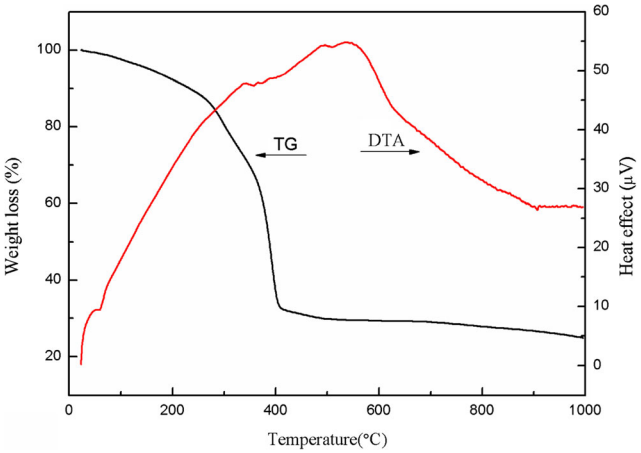


**Fig. 1** TG-DTA analysis curve for the precursor recorded from 40 to 900 °C at the heating rate of 5 °C $min^{-1}$ in Ar atmosphere

### Physical characterization

The structural analysis of the compounds was characterized by X-ray diffraction (XRD, Rint-2000, Rigaku) analysis equipped with Cu-Kα radiation by step scanning in the $2\theta$ range of 10° to 80°. The morphology of the samples was examined by a scanning electron microscope (SEM, JSM-6380 LV) and a Tecnai G12 transmission electron microscope (TEM). Energy-dispersive spectroscopy (EDS) analysis was obtained with the JSM-6380 LV microscope. The carbon content of the sample was confirmed using C-S analysis equipment (Eltar, Germany). Thermal analysis of the sample was determined by TG-DSC equipment (STA-449C, Germany) in argon from room temperature to 900 °C at a heating rate of 5 °C $min^{-1}$.

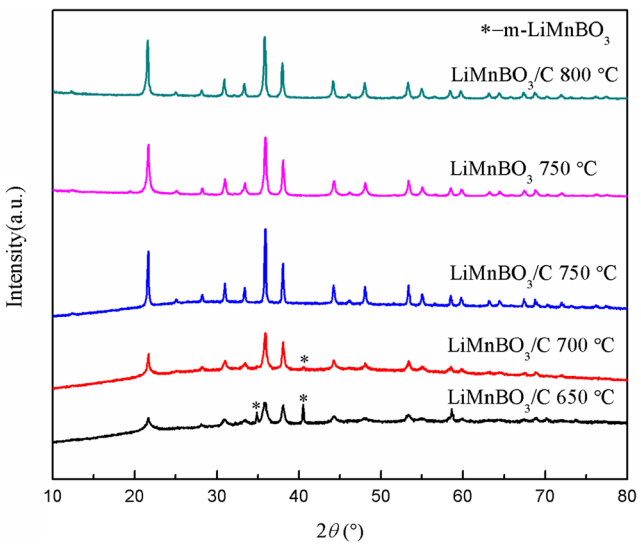


**Fig. 2** XRD patterns of bare $LiMnBO_3$ and $LiMnBO_3$/C samples synthesized at different temperatures

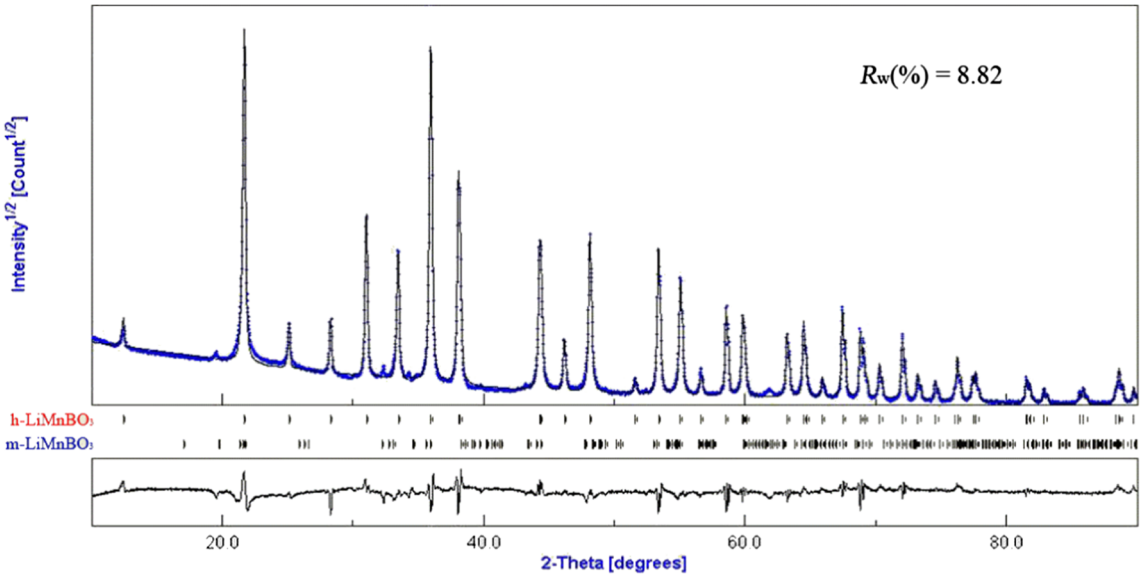


**Fig. 3** Rietveld refinement XRD data of the $LiMnBO_3$/C synthesized at 750 °C

## Electrochemical tests

The electrochemical performance of $LiMnBO_3$/C was characterized by coin-type cells (CR2025) with lithium metal as the negative electrode. The positive electrodes were prepared by mixing $LiMnBO_3$/C, acetylene black, and polyvinylidene fluoride (PVDF) (the weight ratio is 80:10:10) in *N*-methylpyrolline onto an aluminum foil and dried at 120 °C for 4 h in a vacuum oven. Then, the coin-type cells were assembled in a glove box filled with high purity argon. The electrolyte was 1 M $LiPF_6$ solution in a mixture of ethylene carbonate and dimethyl carbonate with 1:1 volumetric ratio. The cells were tested in the voltage range of 1.0–4.8 V at various charge-discharge rates from 0.025 to 0.5 C at room temperature. The cyclic voltammetry (CV) tests and electrochemical impendence spectrum (EIS) measurements were carried out on a CHI660D electrochemical work station. The CV measurements were performed on $LiMnBO_3$/C electrodes at the scanning rate of 0.05 mV $s^{-1}$ from 1.0 to 4.8 V. The EIS measurements were performed in the frequency range of 0.01 Hz–100 kHz with an AC voltage of 5 mV.

## Results and discussion

Figure 1 shows the TG-DTA curves of the precursor powder of $LiMnBO_3$/C. There are three weight loss regions in the TG curve. The first weight loss zone before 240 °C corresponds to the release of molecular water. The second weight loss region (240–350 °C) is mainly attributed to the decomposition of $Mn(CH_3COO)_2$ and PEG. A continuous weight loss between 350 and 500 °C should be related to the reaction of carbon with residue oxygen. No more weight loss is observed in the temperature range from 700 to 900 °C. According to the result, we choose 650, 700, 750, and 800 °C as the heating temperatures to synthesize the $LiMnBO_3$/C composite.

Figure 2 shows the XRD patterns of bare $LiMnBO_3$ and $LiMnBO_3$/C composites synthesized at different temperatures. It is obvious to see that the $LiMnBO_3$/C synthesized at 650 and 700 °C, the hexagonal phase is the dominate phase, but a small amount of monoclinic phase at 34.8° and 40.4°. In addition, the amount of m-$LiMnBO_3$ is reduced with the increasing sintering temperature. In accordance with previous reports, the h-$LiMnBO_3$ is obtained at higher temperature but m-$LiMnBO_3$ is formed at lower temperature [17]. From Fig. 2, it can be seen that the diffraction peaks in the patterns of $LiMnBO_3$/C (synthesized at 750 °C) and $LiMnBO_3$ can be well matched with the h-$LiMnBO_3$. The diffraction peaks of carbon are not detected, which indicates that the carbon generated from PEG is amorphous.

Rietveld refinement is performed to analyze the crystal structure and phase content of the samples, and the results are shown in Fig. 3 and Table 1. From Table 1, the calculated

**Table 1** Results of phase content analysis obtained from X-ray Rietveld refinement

| Sample | Phase content (wt%) | | $R_w$ (%) |
|---|---|---|---|
| | h-$LiMnBO_3$ | m-$LiMnBO_3$ | |
| $LiMnBO_3$/C (650 °C) | 79.45 ± 1.25 | 20.55 ± 0.97 | 10.63 |
| $LiMnBO_3$/C (700 °C) | 90.23 ± 1.89 | 9.77 ± 1.12 | 9.79 |
| $LiMnBO_3$/C (750 °C) | 99.84 ± 0.11 | 0.16 ± 0.09 | 8.82 |
| $LiMnBO_3$ (750 °C) | 99.87 ± 0.09 | 0.13 ± 0.07 | 8.14 |
| $LiMnBO_3$/C (800 °C) | 0 | 100 | 6.25 |

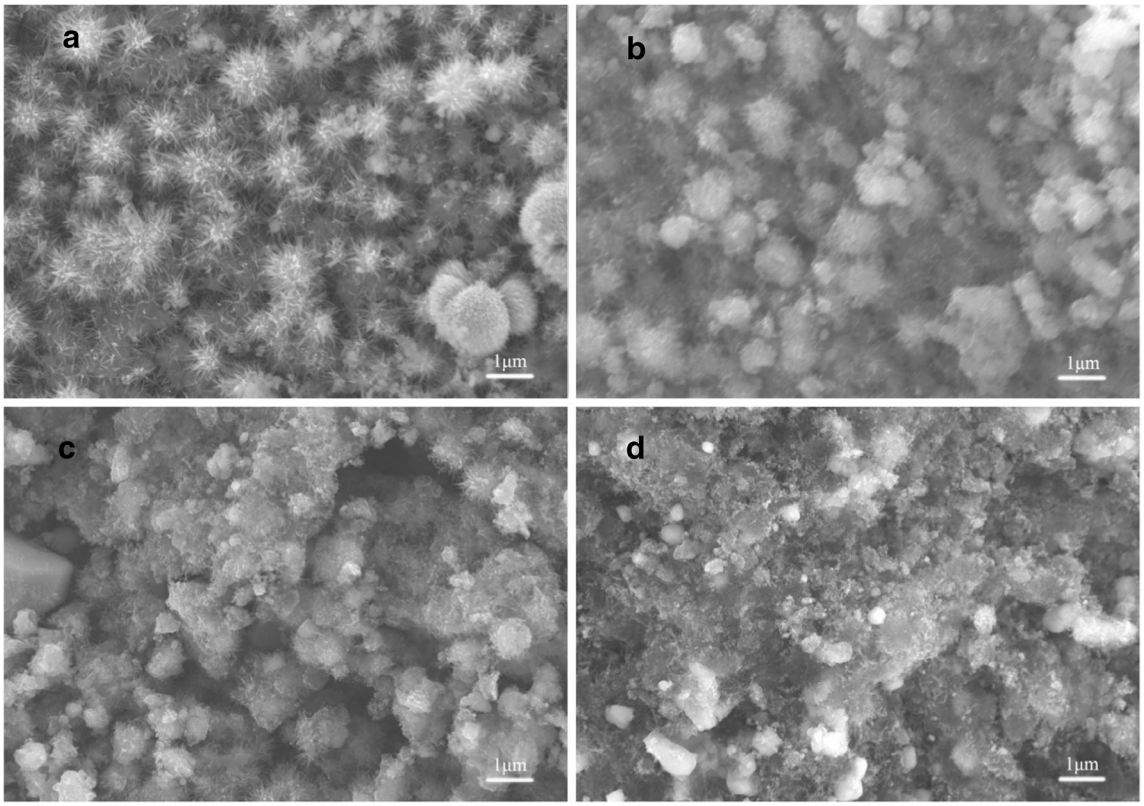


**Fig. 4** SEM images of $LiMnBO_3$/C samples: 650 °C (**a**), 700 °C (**b**), 750 °C (**c**), and 800 °C (**d**)

weight percent of h-$LiMnBO_3$ and the m-$LiMnBO_3$ of $LiMnBO_3$/C synthesized at 750 °C is about 99.84 and 0.16 wt%, respectively. In Fig. 3, a hexagonal phase (ICSD no. 1511217) with P-6 space group can be observed, and the structure is crystallized well for the reliability factor ($R_w$) is good. The calculated and measured $2\theta$ values are well matched. In accordance with the refinement results, the lattice parameters of h-$LiMnBO_3$ are $a$ = 8.1740 Å, $c$ = 3.1489 Å, $V$ = 182.20 Å$^3$, $\alpha = 90°$, $\beta = 90°$, and $\gamma = 120°$, compared well with the reported ones by Zhiping Lin ($a$ = 8.1720 Å, $c$ = 3.1473 Å, $V$ = 182.02 Å$^3$, $\alpha = 90°$, $\beta = 90°$, $\gamma = 120°$) [13].

Figure 4 shows the scanning electron microscopy (SEM) images of the $LiMnBO_3$/C samples. From Fig. 4a–c, we can see that the samples all consist of urchin-like and spherical-like particles. As the annealing temperature is increased, the amount of the urchin-like particles is reduced and the amount of the spherical-like particles is increased; when the annealing temperature is raised to 800 °C, all particles become spherical-like with a particle size of about 1 μm in Fig. 4d. Moreover, to analyze the uniformity of element distribution for $LiMnBO_3$/C, energy-dispersive spectrometry was carried out (Fig. 5). Oxygen, manganese, and carbon are distributed on the various parts of the particles (synthesized at 650 °C), it is clear that carbon are uniformly distributed in the $LiMnBO_3$/C sample. Combined with the XRD results, it can be speculated that the urchin-like particles are m-$LiMnBO_3$ and the spherical-like particles are h-$LiMnBO_3$.

The morphology and microstructure of $LiMnBO_3$ and $LiMnBO_3$/C (synthesized at 750 °C) were characterized by SEM and TEM. As shown in Fig. 6a, the bare $LiMnBO_3$ particles with an average size of ~2 μm are aggregated to form secondary particles. In Fig. 6b, the average particle size of $LiMnBO_3$ in the composite is much smaller than that of bare

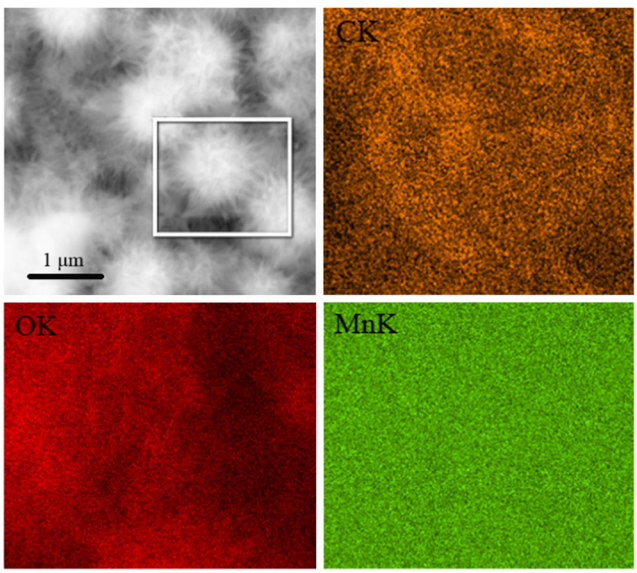


**Fig. 5** EDS images of oxygen, manganese, and carbon for $LiMnBO_3$/C synthesized at 650 °C

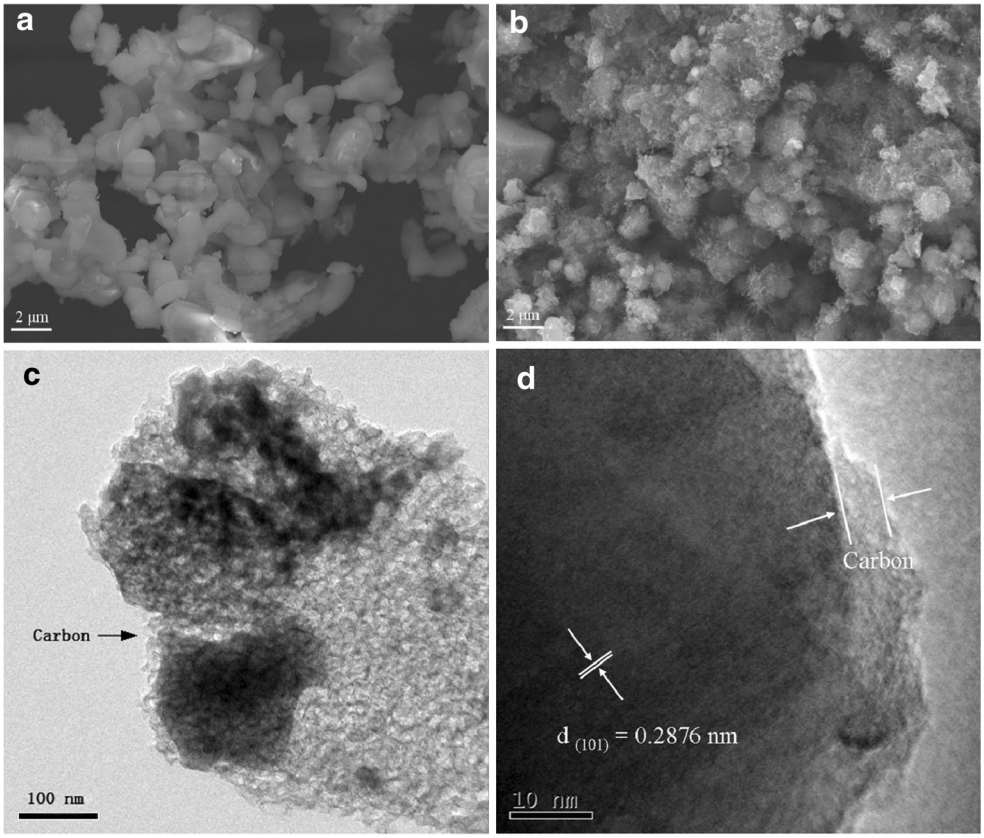


**Fig. 6** SEM images of $LiMnBO_3$ (**a**) and $LiMnBO_3$/C synthesized at 750 °C (**b**). TEM images of $LiMnBO_3$/C synthesized at 750 °C (**c**) and (**d**)

$LiMnBO_3$, due to the confinement of the conductive carbon network. Figure 6c shows the $LiMnBO_3$/C particles (synthesized at 750 °C) are well wrapped with a nano-carbon layer. Figure 6d shows that the interior planar distance between the adjacent lattice fringes is 0.2876 nm, which corresponds to the d-spacing value of the (101) plane of h-$LiMnBO_3$, and the thickness of the carbon coating in the external surface which is beneficial for the electrolyte to permeate into the electrode. Therefore, this structure may be conducive to the insertion/extraction of $Li^+$ from the $LiMnBO_3$ electrode, and the electronic conductivity of $LiMnBO_3$ will be greatly improved.

Figure 7 shows the first charge-discharge curves of the $LiMnBO_3$/C samples synthesized at different temperatures. The cells were all charged at 0.025 C (1 C = 220 mA $g^{-1}$) rate. The initial discharge capacities of samples synthesized at 650, 700, 750, and 800 °C are 135.4, 187.8, 213.4, and 169.9 mAh $g^{-1}$, respectively. The sample synthesized at 750 °C has the highest capacity. The samples calcined at 650 and 700 °C show lower capacities owing to the lower crystallinity. The sample sintered at 800 °C also exhibits a lower capacity due to the bigger particle size and agglomeration which will lengthen the $Li^+$ diffusion/conduction path.

Figure 8a, b shows the first charge-discharge curves of $LiMnBO_3$/C (synthesized at 750 °C) and bare $LiMnBO_3$ cell in the voltage range between 1.0 and 4.8 V at different rates. The first discharge capacities of $LiMnBO_3$/C at 0.025, 0.05, 0.1, 0.2, and 0.5 C are 213.4, 170.8, 128.6, 114.8, and 109.7 mAh $g^{-1}$, respectively. While the bare $LiMnBO_3$ can only deliver 118.5, 105.5, 95.4, 90.8, and 65.6 mAh $g^{-1}$ at the same condition. Figure 8c shows the cycling performance of $LiMnBO_3$/C (synthesized at 750 °C) at different rates. It can be seen that the $LiMnBO_3$/C sample has displayed better cycling performance than bare $LiMnBO_3$. After 50 cycles, the

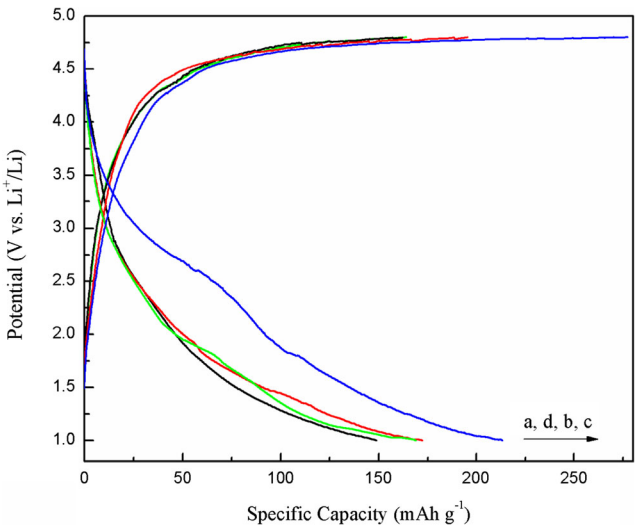


**Fig. 7** First charge-discharge curves of $LiMnBO_3$/C samples at 0.025 C rate, 650 °C (**a**), 700 °C (**b**), 750 °C (**c**), and 800 °C (**d**)

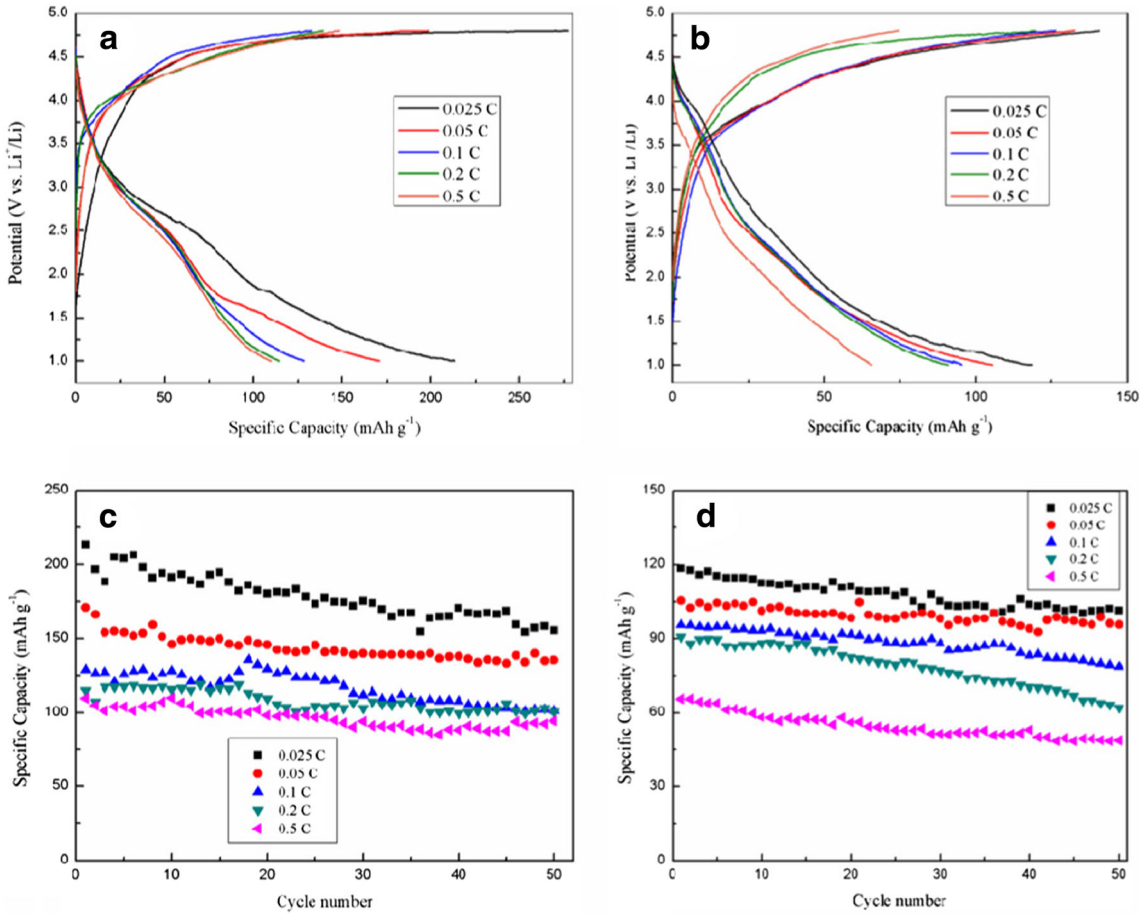


**Fig. 8** First charge-discharge curves of $LiMnBO_3$/C (**a**) and bare $LiMnBO_3$ (**b**) synthesized at 750 °C. Cycle performance of $LiMnBO_3$/C (**c**) and bare $LiMnBO_3$ (**d**) synthesized at 750 °C

discharge capacities of $LiMnBO_3$/C are 155.2, 135.2, 101.2, 100.6, and 94.3 mAh $g^{-1}$, respectively, delivering much higher specific capacities than those of bare $LiMnBO_3$ (Fig. 8d). In fact, the surface of the $LiMnBO_3$ material is very sensitive to the moist air, which tends to induce severe degradation of electrode properties. In our experiment, the in-situ carbon coating from decomposition of the PEG-6000 can prevent $LiMnBO_3$ from contacting with moist air and resist corrosion by the acidic electrolyte during cycling. In addition, the

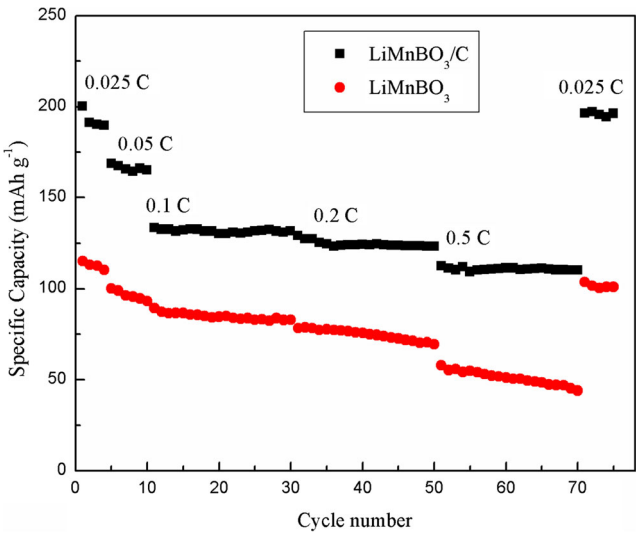


**Fig. 9** Rate capacity of $LiMnBO_3$/C and bare $LiMnBO_3$ synthesized at 750 °C

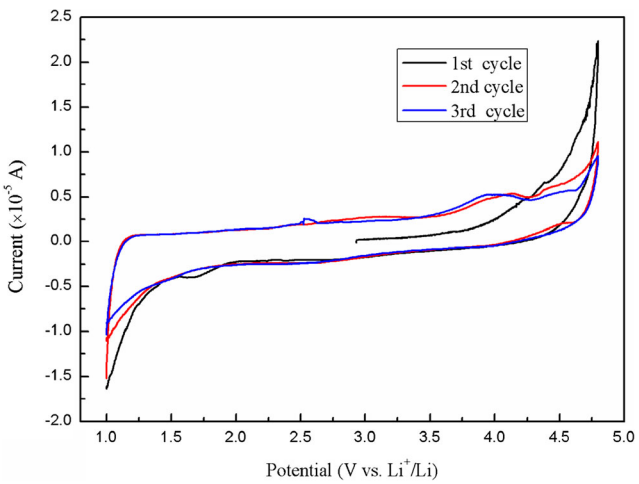


**Fig. 10** Cyclic voltammetry curve of $LiMnBO_3$/C (750 °C) at a scan rate of 0.05 mV $s^{-1}$ in the potential range of 1.0–4.8 V

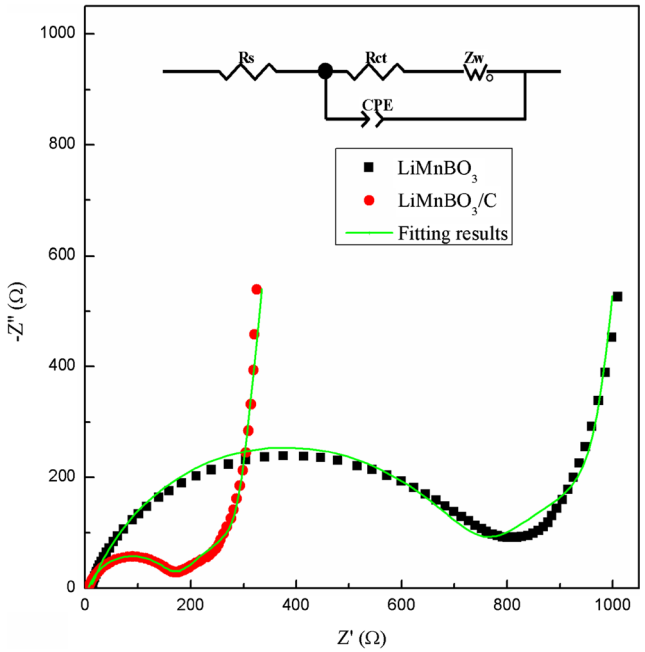


**Fig. 11** EIS spectra of $LiMnBO_3$/C (750 °C) and bare $LiMnBO_3$

electronic conductivity and ionic conductivity can be also improved.

Figure 9 shows the rate capability of $LiMnBO_3$/C (synthesized at 750 °C) and bare $LiMnBO_3$. The current rates are in the range of 0.025, 0.05, 0.1, 0.2, and 0.5 C in sequence for 4, 6, 20, 20, and 20 cycles, respectively. The initial discharge capacities of $LiMnBO_3$/C are 200.1, 168.7, 133.4, 129.2, and 112.6 mAh $g^{-1}$, respectively. After 70 cycles, the current rate returned back to 0.025 C, a capacity of 196.6 mAh $g^{-1}$ still remained. However, the $LiMnBO_3$ can only deliver a capacity of 78.2 mAh $g^{-1}$ at 0.2 C and 57.8 mAh $g^{-1}$ at 0.5 C. The $LiMnBO_3$/C exhibits better rate capability than bare $LiMnBO_3$. The excellent electrochemical performance of $LiMnBO_3$/C composites could be attributed to the intimate imbedding of the particles into the conductive carbon network and electrolyte adsorption in amorphous carbon layer also provided a flexible structure against volume expansion/contraction during the cycling progress. The growth of $LiMnBO_3$ particles is also confined in the sintering process by the carbon network, therefore, lithium ion and electron transport is promoted.

Although, the in-situ carbon coating decreases the capacity loss, the capability rate of $LiMnBO_3$/C is not so excellent, several factors may cause this problem: first, $Mn^{2+}$ may be dissolved into the electrolyte, as similar as the $LiMnPO_4$; second, the $LiMnBO_3$ particles may be separated from the carbon network by the SEI impedance membrane; and last, the particles may be also not small enough for a fully reversible delithiation/lithiation.

Figure 10 shows the CV curves of the $LiMnBO_3$/C (synthesized at 750 °C) at the scanning rate of 0.05 mV $s^{-1}$ in 1.0–4.8 V. A wider oxidation peak can be observed around 4.1 V, ranging from 3.4 to 4.4 V in each cycle, while the corresponding reduction peak does not appear in the reduction process. The intensities of the oxidation peak mildly drop at each cycle corresponding to the capacity loss observed in the charge-discharge curves. The peak potentials almost have little change, suggesting reversible insertion/extraction during cycling. Through the previous report, the low electrical conductivity, dissolution of Mn, and small Li-ion diffusivity of $LiMnBO_3$ led to the CV curves with sharp and symmetrical redox peaks difficultly [30].

The EIS tests (Fig. 11) were comparatively conducted to investigate the electrical conductivity of bare $LiMnBO_3$ and $LiMnBO_3$/C synthesized at 750 °C. The EIS spectrums exhibit a semicircle in the high frequency range and an inclined line in the low frequency range. Using the Z-view software, EIS data can be fitted by an equivalent circuit model, and some parameters are tabulated in Table 2. An equivalent circuit (insert figure) was conducted to refine the spectra. $R_s$ represents the resistance of the electrolyte as the intercept impedance on the Z′ axis, $R_{ct}$ is the charge transfer resistance, $Z_w$ is the Warburg impedance arising from the $Li^+$ diffusion in electrode, corresponding to the inclined line. CPE represents the double-layer capacitance. It is found that the charge transfer resistance of $LiMnBO_3$/C (153.6 Ω) is much lower than that of bare $LiMnBO_3$ (716.6 Ω), indicating the charge transfer speed of the electrochemical reaction is significantly increased. The exchange current density ($j_0$) is calculated by the following equation. The results are also shown in Table 2.

$$j_o = \frac{RT}{nFR_{ct}}$$

Where $R$ is the gas constant, $T$ is the absolute temperature, $n$ is the number of electrons involved in the redox process, $F$ is Faraday's constant, and $R_{ct}$ is the charge transfer resistance. The exchange current density ($j_0$) of $LiMnBO_3$/C ($1.67 \times 10^{-4}$ mA $cm^{-2}$) is about one order magnitude higher than that of bare $LiMnBO_3$ ($3.59 \times 10^{-5}$ mA $cm^{-2}$), which indicates that the reversibility of the electrode reaction of $LiMnBO_3$/C is much better than that of $LiMnBO_3$.

**Table 2** Parameters obtained from equivalent circuit fitting of experimental data

| Sample | $R_s$ (Ω) | $R_{ct}$ (Ω) | $j_o$ (mA $cm^{-2}$) |
|---|---|---|---|
| $LiMnBO_3$ (750 °C) | 10.69 | 716.60 | $3.59 \times 10^{-5}$ |
| $LiMnBO_3$/C (750 °C) | 5.04 | 153.60 | $1.67 \times 10^{-4}$ |

## Conclusions

$LiMnBO_3$/C cathode materials were successfully prepared by a sol-gel method using PEG as the reductive agent and carbon source. $LiMnBO_3$/C synthesized at 750 °C shows excellent electrochemical performance with the discharge capacities of 155.2, 135.2, and 94.3 mAh $g^{-1}$ after 50 cycles at 0.025, 0.05, and 0.5 C rates, respectively, exhibiting a much better cycling performance than that of bare $LiMnBO_3$. The enhancement of the electrochemical performance of $LiMnBO_3$/C could be attributed to the homogeneous coating of the carbon network, which can not only improves the electronic conductivity of $LiMnBO_3$ but also boosts the $Li^+$ diffusion.

**Acknowledgements** This study was supported by the National Natural Science Foundation of China (51574168, 51574170, and 51404156), Natural Science Foundation of Jiangsu Province of China (BK20141231), and Science and Technology Plan Projects of Suzhou, China (SYG201512).

## References

1. Legagneur V, An Y, Mosbah A, Portal R, Salle ALL, Verbaere A, Guyomard D, Piffard Y (2001) $LiMBO_3$ (M = Mn, Fe, Co): synthesis, crystal structure and lithium deinsertion/insertion properties. Solid State Ionics 139:37–46
2. Chen L, Zhao YM, An XN, Liu JM, Dong YZ, Chen YH, Kuang Q (2010) Structure and electrochemical properties of $LiMnBO_3$ as a new cathode material for lithium-ion batteries. J Alloys Compd 494:415–419
3. Roux BL, Bourbon C, Lebedev OI, Colin JF, Pralong V (2015) Synthesis and characterization of the $LiMnBO_3$-$LiCoBO_3$ solid solution and its use as a lithium-ion cathode material. Inorg Chem 54: 5273–5279
4. Barpanda P, Dwibedi D, Ghosh S, Kee Y, Okada S (2015) Lithium metal borate ($LiMBO_3$) family of insertion materials for Li-ion batteries: a sneak peak. Ionics 21:1801–1812
5. Ragupathi V, Safiq M, Panigrahi P, Hussain T, Raman S, Ahuja R, Nagarajan GS (2017) Enhanced electrochemical performance of $LiMnBO_3$ with conductive glassy phase: a prospective cathode material for lithium-ion battery. Ionics. doi:10.1007/s11581-017-2019-8
6. Kim JC, Moore CJ, Kang B, Hautier G, Jain A, Ceder G (2011) Synthesis and electrochemical properties of monoclinic $LiMnBO_3$ as a Li intercalation material. J Electrochem Soc 158:A309–A315
7. Muslim A, Ting M, Zhi S, Ili N (2014) Structural feature and electrochemical performance of h-$LiMnBO_3$ and its carbon coated material prepared by microwave synthesis. Rare Metal Mat Eng 43: 2095–2099
8. Zhao LW, Li RK (2013) Study on a multifunctional crystal $LiMnBO_3$. Mater Res Bull 48:277–280
9. Lee YS, Lee H (2014) Structure and electrochemical behavior of $LiMnBO_3$ synthesized at various temperatures. Electron Mater Lett 10:253–258
10. Veena R, Shanmukaraj D, Ganapathi SN, Sudarkodi R (2014) Synthesis and morphological influence on high capacity $LiMnBO_3$ cathode material for new generation lithium ion batteries. ECS Trans 62:123–128
11. Tao L, Neilson JR, Melot BC, McQueen TM, Masquelier C, Rousse G (2013) Magnetic structures of $LiMBO_3$ (M=Mn, Fe, Co) lithiated transition metal borates. Inorg Chem 52:11966–11974
12. Li SL, Xu LQ, Li GD, Wang M, Zhai YJ (2013) In-situ controllable synthesis and performance investigation of carbon-coated monoclinic and hexagonal $LiMBO_3$ composites as cathode materials in lithium-ion batteries. J Power Sources 236:54–60
13. Lee KJ, Kang LS, Uhm SY, Yoon JS, Kim DW, Hong HS (2013) Synthesis and characterization of $LiMnBO_3$ cathode material for lithium ion batteries. Curr Appl Phys 13:1440–1443
14. Kim JC, Li X, Moore CJ, Bo SH, Khalifah PG, Grey CP, Ceder G (2014) Analysis of charged state stability for monoclinic $LiMnBO_3$ cathode. Chem Mater 26:4200–4206
15. Lin ZP, Zhao YJ, Zhao YM (2012) First-principles study of the structural, magnetic, and electronic properties of $LiMBO_3$ (M=Mn, Fe, Co). Phys Lett A 376:179–184
16. Karthikeyan K, Lee Y (2014) Microwave synthesis of high rate nanostructured $LiMnBO_3$ with excellent cyclic behavior for lithium ion batteries. RSC Adv 4:31851–31854
17. Tang AP, He DH, He ZQ, Xu GR, Song HS, Peng RH (2015) Electrochemical performance of $LiMnBO_3$/C composite synthesized by a combination of impregnation and precipitation followed by annealing. J Power Sources 275:888–892
18. Ma R, Shao LY, Wu KQ, Lao MM, Shui M, Chen C, Wang DJ, Long NB, Ren YL, Shu J (2013) Electrochemical behaviors of hexagonal $LiMnBO_3$ as lithium storage host material for lithium-ion batteries. Ceram Int 39:9309–9317
19. Lee YS, Lee H (2014) Improved lithium storage capacities of $LiMnBO_3$/C via simple high-energy milling. Mater Lett 132:401–404
20. Zhang B, Ming L, Zheng JC, Zhang JF, Shen C, Han YD, Wang JL, Qin S (2014) Synthesis and characterization of multi-layer core-shell structural $LiFeBO_3$/C as a novel Li-battery cathode material. J Power Sources 261:249–254
21. Zheng JC, Han YD, Sun D, Zhang B, Cairns EJ (2017) In situ-formed $LiVOPO_4$@$V_2O_5$ core-shell nanospheres as a cathode material for lithium-ion cells. Energy Storage Mater 7:48–55
22. Zheng JC, Qin SE, Zhang B, Ou X, Ming L, Shen C, Han YD, Wang JL, Zhang JF (2014) $LiMnBO_3$/carbon composite material synthesized by ball-milling and postannealing. Chem Lett 43:1411–1413
23. Yamada A, Iwane N, Nishimura SI, Koyama Y, Tanaka I (2011) Synthesis and electrochemistry of monoclinic $Li(Mn_xFe_{1-x})BO_3$: a combined experimental and computational study. J Mater Chem 21: 10690–10696
24. Zhong SK, Chen W, Wu L, Liu JQ (2012) A PEG-assisted rheological phase reaction synthesis of $5LiFePO_4{\cdot}Li_3V_2(PO_4)_3$/C as cathode material for lithium ion cells. Ionics 18:523–527
25. Nien YH, Carey JR, Chen JS (2009) Physical and electrochemical properties of $LiFePO_4$/C composite cathode prepared from various polymer-containing precursors. J Power Sources 193:822–827
26. Yun NJ, Ha HW, Jeong KH, Park HY, Kim K (2006) Synthesis and electrochemical properties of olivine-type $LiFePO_4$/C composite cathode material prepared from a poly(vinyl alcohol)-containing precursor. J Power Sources 160:1361–1368
27. Gong C, Deng F, Tsui CP, Xue Z, Ye Y, Tang CY, Zhou X, Xie X (2014) PANI-PEG copolymer modified $LiFePO_4$ as a cathode material for high-performance lithium ion batteries. J Mater Chem 2: 19315–19323
28. Yang Y, Liao XZ, Ma ZF (2009) Superior high-rate cycling performance of $LiFePO_4$/C-PPy composite at 55 C. Electrochem Commun 11:1277–1280
29. Stafeevaz VS, Drozhzhin OA, Panin RV, Filimonov DS, Fabrichnyi PB, Yashina LV, Khasanova NR, Antipov EV (2015) The effect of $LiFeBO_3$/C composite synthetic conditions on the quality of the cathodic material for lithium-ion batteries. Russ J Electrochem 51:619–626

30. Afyon S, Kundu D, Krumeich F, Nesper R (2013) Nano-$LiMnBO_3$, a high-capacity cathode material for Li-ion batteries. J Power Sources 224:145–151
31. Zhang B, Zhu YS, Yu WJ, Zhang JF, An CS (2017) Facile synthesis of carbon-encapsulated $LiMnBO_3$ composite by the sol-gel method as a lithium-ion battery cathode material. J Alloys Compd 704:343–347
32. Ma T, Muslim A, Su Z (2015) Microwave synthesis and electrochemical properties of lithium manganese borate as cathode for lithium ion batteries. J Power Sources 282:95–99